Journal of Rock Mechanics and Geotechnical Engineering 14 (2022) 770–780

Contents lists available at ScienceDirect

Journal of Rock Mechanics and Geotechnical Engineering

journal homepage: www.jrmge.cn

Full Length Article

Improved uranium leaching efficiency from low-permeability sandstone using low-frequency vibration in the CO_2+O_2 leaching process

Yong Zhao [a,b,*], Yong Gao [c], Caiwu Luo [a], Jun Liu [d]

[a] School of Resource Environment and Safety Engineering, University of South China, Hengyang, 421001, China
[b] Department of Nuclear Safety, China Institute of Atomic Energy, Beijing, 100000, China
[c] College of Humanities and Foreign Languages, Xi'an University of Science and Technology, Xi'an, 710054, China
[d] China Coal Technology Engineering Group Chongqing Research Institute, Chongqing 400039, China

ARTICLE INFO

Article history:
Received 22 March 2021
Received in revised form
21 July 2021
Accepted 18 October 2021
Available online 30 December 2021

Keywords:
Uranium leaching
Low-frequency vibration
Chemical erosion
Low permeability
Permeability model

ABSTRACT

Extraction of uranium from low-permeability sandstone is a long-standing challenge in mining. The improvement of sandstone permeability has therefore become a key research focus to improve the uranium leaching effect. To address the low-permeability problem and corresponding leaching limits, leaching experiments are performed using newly developed equipment that could apply low-frequency vibration to the sandstone samples. The test results indicate that low-frequency vibration significantly improves the uranium leaching performance and permeability of the sandstone samples. The leaching effect of low-frequency vibration treatment is approximately nine times more effective than ultrasonic vibration treatment, whereas the concentration of uranium ions generated without vibration treatment is not detectable. Mathematical model that considers the combined action of physico-mechanical vibration and chemical erosion is established to describe the effect of low-frequency vibration on the permeability. The calculated results are in good agreement with the tested permeability values. This study thus offers a new method to effectively leach more uranium from low-permeability sandstone using CO_2+O_2 and provides an insight into the impact of low-frequency vibration on the uranium leaching process.

1. Introduction

Worsening environmental pollution has led industrial nations to focus on the development and use of nuclear power. The annual demand for natural uranium by nuclear power plants worldwide was estimated to be 77,000 tons in 2020 and is expected to reach 90,000 and 110,000 tons by 2025 and 2030, respectively. In China, more than 70% of sandstone-type uranium mineral resources occur in compact sandstone reservoirs with low permeability (Yuan et al., 2018). Easily exploited uranium resources have already been extensively mined; thus, an increasing amount of research has focused on uranium mining from low-permeability deposits to meet the uranium demand for nuclear power production. CO_2+O_2 neutral leaching is often used in production to minimize groundwater environmental pollution during the leaching process (Mudd, 2001). CO_2+O_2 leaching methods have mainly been aimed at sandstone with optimal permeability, but lower-porosity sandstone layers have fewer channels through which the leaching solution can pass. Lower-permeability sandstone generates a smaller amount of leached uranium, which is not conducive to in situ leaching mining. The key to increase the amount of leached uranium is thus to effectively improve the permeability of low-permeability sandstone during the uranium leaching process (Yuan et al., 2018).

Previous measures to enhance leaching effects have included blasting explosion (Yuan et al., 2018), surfactants (Cai et al., 2013; Tan et al., 2014; Ai et al., 2019; Du et al., 2019; Pan et al., 2020), vibration waves, microwaves (Cho et al., 2020; Laubertova et al., 2020), electro-assisted leaching (Deng et al., 2019; Tian et al., 2019; Li et al., 2020), and bio-oxidative leaching (Wang et al., 2013; Yang et al., 2020) modes. Among these, vibration waves have been studied in the form of ultrasonic and low-frequency vibrations. Ultrasonic waves are mechanical vibration type with frequencies above 20 kHz that are excited by a vibration source in

* Corresponding author. School of Resource Environment and Safety Engineering, University of South China, Hengyang, 421001, China.
E-mail address: 2015002103@usc.edu.cn (Y. Zhao).

Peer review under responsibility of Institute of Rock and Soil Mechanics, Chinese Academy of Sciences.

https://doi.org/10.1016/j.jrmge.2021.10.013

an elastic medium. The main mechanism of the sonochemical reaction is cavitation generated by ultrasonic waves in solution, which leads to a thermodynamic change of the chemical reaction and improves the reaction rate and leaching. With respect to uranium leaching, Avvaru et al. (2006, 2008) showed that the use of ultrasound notably improves the leaching rate of uranium within the investigated leach acid media. Ladola et al. (2014) found that the recovery of uranium from MgF_2 slag is improved owing to ultrasonic treatment and the acoustic cavitation is more effective on larger sized ore particles. With respect to the leaching of other metals, ultrasound treatment has been shown to improve the leaching rate of gold from refractory gold ores (Zhu et al., 2012), nickel from nickel laterite ore (Chen et al., 2015), zinc from low-grade zinc oxide ore (Li et al., 2015), germanium from roasted slag containing germanium (Zhang et al., 2016a), copper from copper-bearing tailings (Zhang et al., 2008a), tungsten from scheelite concentrate (Zhao et al., 2013), rare earth elements from concentrated nickel sulfide (Xue et al., 2010), silver from a spent symbiosis lead-zinc mine (Li et al., 2018a), vanadium from shale (Chen et al., 2020), copper from chalcopyrite (Wang et al., 2020), and potassium from phosphorus-potassium associated ore (Zhang et al., 2016b). Previous ultrasonic vibration studies mainly focused on powdered ore; however, the actual in situ leaching process involves low-permeability block ore. Previous conclusions regarding ultrasonic leaching may therefore not be applicable to the in situ leaching of low-permeability uranium-bearing sandstone. Although low-frequency vibration has been widely applied in the oil industry to increase oil permeability (Sun et al., 2020), its use in uranium leaching has only been reported by Makaryuk (2009). The application of low-frequency vibration in the field improves the extent of particle blockage in a sandstone layer and modifies the water head. However, a change of the water head may be related to a blockage change caused by (i) the loss of wall-protecting mud from the boreholes into the ore-bearing aquifer, (ii) the formation of rock powder pressed into the ore-bearing aquifer during the drilling process, or (iii) a change of the natural permeability, which cannot be used to directly explain the effective improvement of the natural sandstone permeability owing to vibration. Furthermore, Makaryuk (2009) did not report the type of injected leaching agent used in their study, as well as the effect of vibration on the leaching agent. The key factors for mining in low-permeability sandstone include an improvement of the rock self-permeability, the leaching agent, and the influence of vibration on the leaching agent. It is therefore necessary to study the influence of low-frequency vibration treatment on sandstone self-permeability and leaching effects during the CO_2+O_2 leaching process, and compare the leaching effects of ultrasonic and low-frequency vibrations for low-permeability sandstone.

In this study, low-frequency mechanical vibration is innovatively introduced into the CO_2+O_2 uranium leaching process of low-permeability sandstone. The device specification is first presented, followed by a description of the experimental system. The test procedure and results are then explained and the permeability model is established. This study provides a new method for CO_2+O_2 leaching of low-permeability sandstone.

2. Methods

2.1. Device specification

During the in situ leaching process, leaching solution reacts with the ore and uranium IV oxidizes to uranium VI by reaction with O_2. CO_2 dissolved in the water generates HCO_3^- and both uranium VI and HCO_3^- generate uranyl carbonate ions, which can exist stably in aqueous solution. The specific reaction principles are as follows (Kim et al., 2014; Rao et al., 2014; Sreenivas and Chakravartty, 2016; Asghar et al., 2020; Shen et al., 2020):

$$2UO_2+O_2 = 2UO_3 \quad (1)$$

$$UO_3+2HCO_3^- = [UO_2(CO_3)_2]^{2-}+H_2O \quad (2)$$

$$[UO_2(CO_3)_2]^{2-}+HCO_3^- = [UO_2(CO_3)_3]^{4-}+H^+ \quad (3)$$

Throughout the course of the chemical reaction, the leaching solution flows in the sandstone, which is affected by the primary pore and fracture structure. Erosion owing to the reaction continuously produces pores and fractures in the sandstone interior. This affects the physical seepage process of the leaching solution, which is required for the chemical reaction to proceed. Uranium leaching is therefore influenced by physico-chemical reactions. In terms of physical factors, the uranium leaching rate depends on the extent of change of the sandstone porosity and permeability. In terms of chemical factors, the leaching rate improves by increasing the temperature of the leaching solution and amount of CO_2 and O_2 dissolved in the water. These individual factors during the uranium leaching process must be investigated. The designed experimental device must satisfy the following requirements:

(1) When the CO_2 and O_2 pressure and water volume reach a specific value, the leaching reaction occurs under different temperature, amplitude and frequency conditions.
(2) The leaching reaction occurs over a range of CO_2 and O_2 pressure and water volume conditions at constant temperature, amplitude and frequency.
(3) Two forms of low-frequency and ultrasonic vibration can be realized and the vibration time can be controlled.
(4) The excitation force and pressure within the reaction kettle can be monitored, radon gas produced after the reaction can be measured, and the leaching solution can be easily sampled and measured after the reaction has completed.

2.2. Experimental system

The experimental system for vibration leaching developed in this study comprises six parts: a water and gas supply system, an external reaction device, an excitation system, a signal acquisition system, a radon measuring system, and a vacuum pumping system. A schematic diagram of the full system is shown in Fig. 1.

The water and gas supply system is used to control the reaction materials and is mainly composed of a globe valve, water tank, high-pressure solenoid valve, one-way valve, high-pressure trimming valve, and accessories. Owing to the explosivity of oxygen, the water supply must be applied under normal pressure. The water, carbon dioxide and oxygen are therefore supplied from three separate channels. The reaction kettle is successively filled with water, oxygen and carbon dioxide to control the gas filling pressure and filling gas and water ratio.

The external reaction device provides the reaction location and mainly includes a temperature control device, reaction kettle, elastic support for the reaction kettle, base, inner tank of the reaction kettle, gas pressure sensor, safety valve, filter, and high-pressure ball valve. The temperature is set and monitored using a programmable logic controller touch screen, by which can also control the solenoid valve. The gas inlet and water intake pipelines are connected with the reaction kettle by high-pressure rubber pipes. The base is fixed on the ground by an expansion bolt to reduce the recoil force generated by the vibration exciter during vibration.

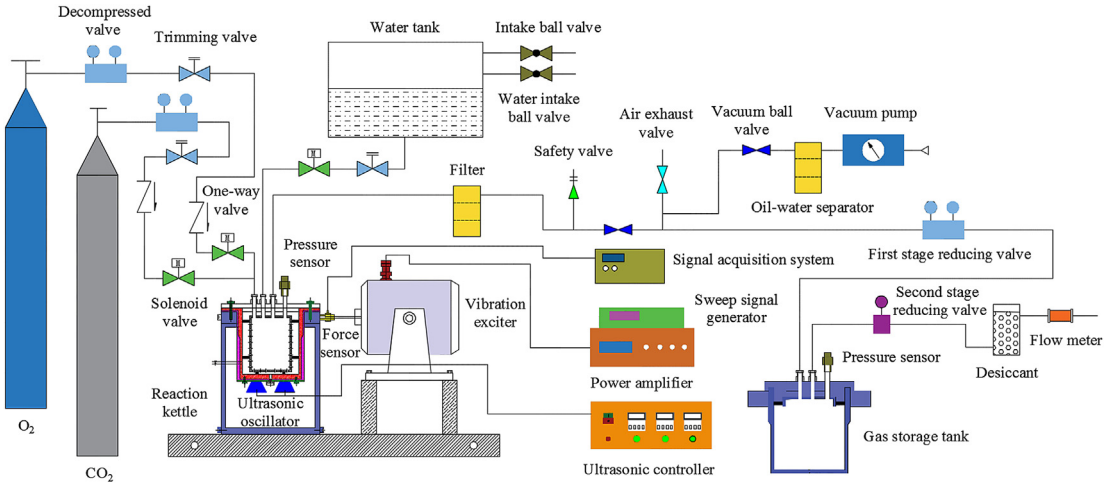

Fig. 1. Testing system for vibration leaching.

The excitation system controls the reaction conditions, which comprises high- and low-frequency vibrating system components. The high-frequency vibration system includes the ultrasonic oscillators and a controller. The ultrasonic oscillator is fixed at the reaction kettle bottom by a flange, and the oscillator of the different frequencies is adjusted by replacing the flange. The low-frequency vibrating system contains a JZK-20 electric vibration exciter, bracket, sweep signal generator, and power amplifier. The vibration exciter and force sensor are connected by a long screw by which the vibration exciter drives the reaction kettle vibration. The sweep signal generator can set the wave shape of the vibration and frequency, and the amplitude is governed by setting the magnifying current of the power amplifier.

The signal acquisition system collects and records the change of excitation force monitored by the force sensor. This system contains a charge amplifier, force sensor, data acquisition device, and computer. The received force signal is transformed into an electric signal by the force sensor attached to the outer wall of the reaction kettle. Amplified by a charge amplifier, the signal is transmitted to the data collector for signal analysis and then recorded by the computer.

The radon measuring system is used to measure radon gas after the reaction, which contains a first-stage pressure reducing valve, gas storage tank, pressure sensor, as well as a second-stage pressure reducing valve, drying tank, flowmeter, and RAD7 radon measurement instrument. The gas flows at very high pressure from the reaction kettle, but the RAD7 radon measurement instrument can only withstand atmospheric pressure. The pressure reducing valve is thus used to protect the radon measurement instrument.

The vacuum pumping system is used for the pretreatment, which comprises a high-pressure ball valve, oil-water separator, vacuum pressure gauge, and vacuum pump. An air exhaust hole with a high-pressure ball valve is fitted on the vacuumed pipeline. After relieving the gas in the reaction kettle, the gas in the pipeline passes through the high-pressure ball valve and enters the oil-water separator to filter out the water. The pipeline is then vacuumed by the pump.

2.3. Experiments

2.3.1. Experimental protocol

The drill core samples were not all low-permeability sandstone. To obtain low-permeability sandstone samples, primary ore from each drill hole was uniformly mixed with calcite and distilled water and compressed. The vibration treatment time was the same for samples prepared from same drill hole primary ore and differed between different drill hole primary ores. The experiments were thus able to discern the effects of vibration frequency on leaching and permeability, while also restoring the actual underground leaching condition as much as possible. Sample leaching at the same frequency and variable treatment time is considered to be a layered leaching sandstone process at various depths. Single samples are thus interpreted as individual sandstone layers and the leaching content of samples with different vibration times over a certain time frame sums to the leaching content of a cumulative layer at that time, which better reflects the practical impacts of vibration on sandstone beds. Drill core samples of uranium ore from different boreholes were individually wrapped in fresh-keeping film, as shown in Fig. 2. For comparison, the uranium leaching content and HCO_3^- concentration were also measured under ultrasonic vibration.

As mentioned, primary ore from the same drill hole was uniformly mixed with calcite and distilled water and compressed to obtain low-permeability sandstone samples. Forty samples were used to compare the leaching changes, including eight samples at each frequency. The HCO_3^- concentration in the leaching solution was measured in all of the samples, in addition to the permeability change and leached ion concentrations under low-frequency vibration, and the sample appearances were compared in terms of

Fig. 2. Drill core samples of uranium ore.

erosion analysis. The vibration treatment time was the same for samples prepared from the same drill hole, but varied between drill holes.

2.3.2. Experimental process

The experimental process involves four steps: Sample preparation, sample installation, reaction control and post-reaction treatment. The specific process is described as follows.

(1) Sample preparation

Low-grade uranium ore was obtained by drilling to a depth of 610 m in a mine. The collected samples were crushed and 312-g ore particles (30–100 mm) were screened, together with a mixture of 104-g calcite (800 mm). During mixing, 30 g of distilled water was added to increase the cohesive force upon shaping. A uniform mixture was loaded into a pressing die and then inserted into the servo press. Cylindrical sample of 50 mm in diameter and 100 mm in height was prepared by servo press acceleration to 204 kN at a rate of 2.4 kN/s and then maintained at this pressure for 20 min. The sample preparation process is shown in Fig. 3.

(2) Permeability measurement

The leaching of low-permeability sandstone is affected by its permeability. Sample permeabilities were therefore measured before and after vibration treatment to assess the effects of vibration and relationship between permeability and leaching. Samples wrapped with fresh-keeping film were placed into the core holder. After pumping under a vacuum for 30 min, the water injection pump was adjusted to ensure that the samples were saturated under constant water pressure until the water pressure value in the front and rear ends of the core holder were equal. The saturated water in the sample was then displaced under constant current until the water pressure in the front end of the core holder stabilized. The water pressure values in the front and rear ends of the core holder and pump flow rate were recorded. The permeability is calculated by Darcy's law.

(3) Control of the reaction process

There are six steps for control of the reaction process described as follows:

(i) Sample installation. Samples with fresh-keeping film were placed in the inner gallbladder and then blanched along the inner gallbladder holes with 14.13-mm vertical row spacing. The hole spacing of 6 mm and aperture diameter of 4 mm were used to ensure uniform contact with the external solution. The inner gallbladder was then placed in the reaction kettle.

(ii) Vacuuming. All valves of the system were closed and two globe valves were opened, which connect with the vacuum pump and reaction kettle. The pressure reducing valve connected with vacuum pump and the gas storage tank was opened. The vacuum pump was then started to pump the reaction kettle and gas storage tank. After 5 min, the pump and all the valves were closed.

(iii) Water injection. The water tank was filled with distilled water. The water intake solenoid valve and trimming valve were opened to inject 1700 mL of water into the reaction kettle. The trimming valve was then closed, followed by the solenoid valve.

(iv) Heating. The temperature controller was set and the heating valve was opened to heat the reaction kettle to 30 °C and the temperature was then held constant.

(v) Gas injection. Oxygen was first injected. When reaching the preset temperature condition, the pressure reducing valve at the front end of the oxygen cylinder was adjusted. The oxygen solenoid valve and oxygen trimming valve were then switched on. Oxygen was injected into the reaction kettle until the pressure reached 1 MPa. The solenoid valve and trimming valve were then closed in sequence. Carbon dioxide was then injected. The pressure reducing valve at the front of the carbon dioxide cylinder, the carbon dioxide solenoid valve and carbon dioxide trimming valve were opened in turn. Carbon dioxide was filled into the reaction kettle until the pressure reached 2 MPa. The solenoid valve and trimming valve were then sequentially closed.

(vi) Vibrating. In the low-frequency vibration experiments, the sweep signal generator and power amplifier were opened so that the exciter drove the reaction kettle to vibrate in accordance with the same force amplitude and different frequencies. In the ultrasonic vibration experiments, the ultrasonic controller was opened to impose ultrasonic vibration on the reaction kettle.

(4) Post-reaction treatment

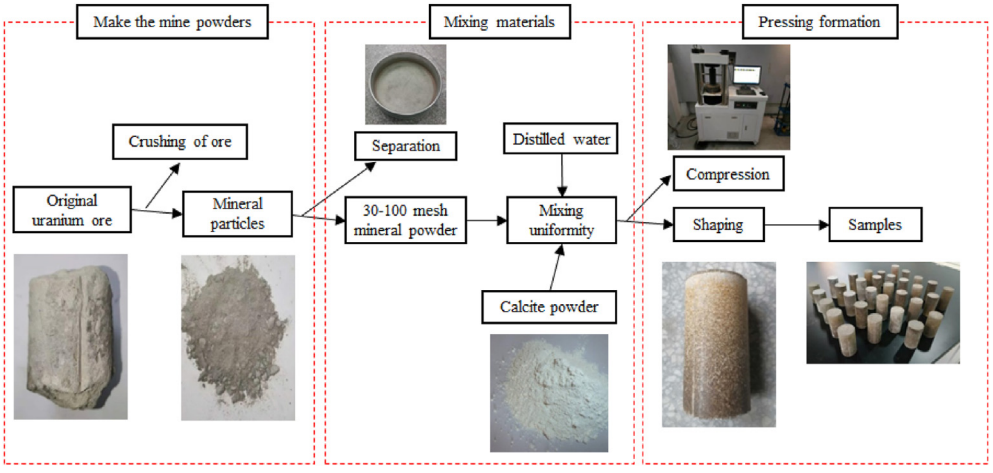

Fig. 3. Sample preparation process.

After vibrating for a specific time, the power amplifier was closed. The pressure reducing valve at the front end of the gas storage tank was set to 0.02 MPa and the pressure reducing valve at the back end was adjusted to secure the flowmeter to less than 1 L/min to protect the radon detector. After the radon was measured, the heating valve was closed and the exhaust valve was opened to discharge the residual gas in the testing system. The pressure reducing valve was then closed. The reaction kettle was then opened, the sample was removed, and the leaching solution was collected.

3. Results and discussion

3.1. Analysis of vibration effect

3.1.1. Effect of vibration treatment on uranium concentration

After the reaction had completed, 300 mL of leaching solution was collected and the uranium concentration in solution was measured via spectrophotometry (Ladola et al., 2014), as shown in Fig. 4a. Uranium ions were detected in solution after 8 h of low-frequency vibration treatment and after 14 h of ultrasonic vibration treatment, but remained undetected in untreated samples after 22 h of leaching. Within 8–22 h of vibration treatment time, the uranium leaching amount increased with low-frequency vibration frequency from 0.049 to 1.35 mg/L at 10 Hz to 0.239–1.609 mg/L at 20 Hz and finally to 0.645–2.36 mg/L at 30 Hz. In contrast, the uranium leaching amount decreased with ultrasonic vibration frequency from 0.062 to 0.257 mg/L at 28 kHz to 0.051–0.205 mg/L at 40 kHz. This is mainly because lower ultrasonic vibration frequencies produce larger bubble radii, higher pressure and energy within the bubbles, and stronger ultrasonic cavitation (Ye et al., 2019). In addition, the power of the 10 Hz vibration was 30 W, compared with 100 W for the 28 kHz and 40 kHz vibrations. The results demonstrate that low-frequency vibration treatment significantly improves uranium leaching and to a higher degree outperforms the ultrasonic vibration treatment.

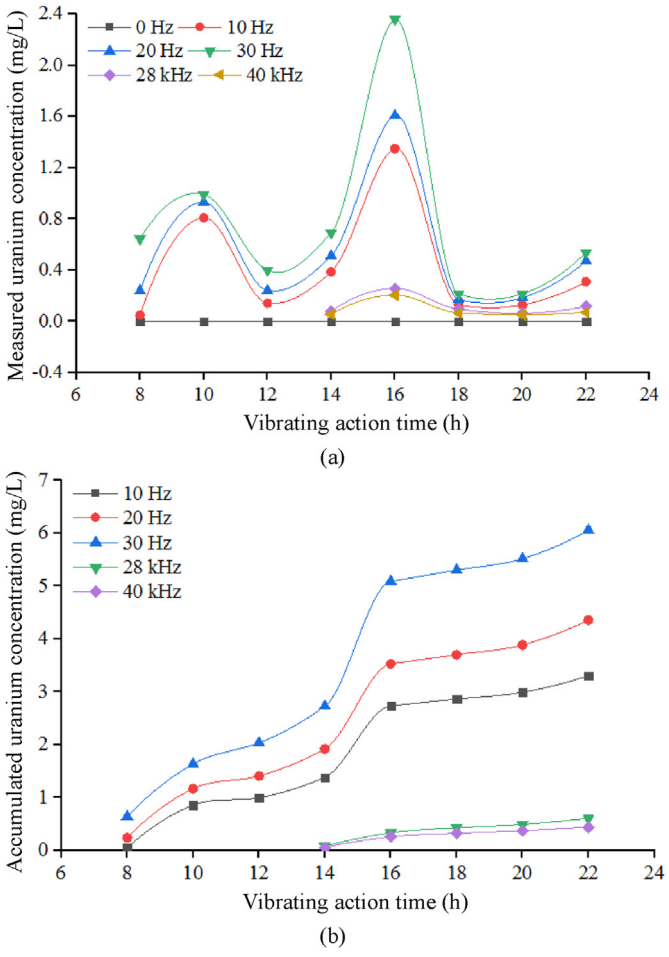

Fig. 4. Changes of (a) measured and (b) accumulated uranium concentrations from vibration leached sandstone samples.

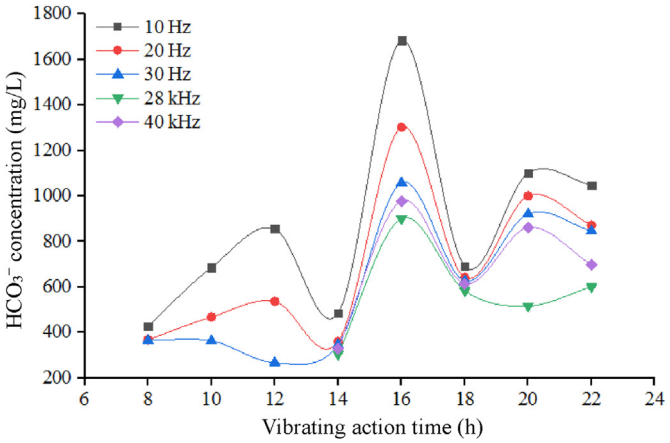

Fig. 5. HCO_3^- concentration in solution variations from the vibration-treated leached sandstone samples.

The leaching process of samples for different treatment times at the same frequency is considered a layer leaching process with different burial depths of sandstone under the same frequency. The uranium concentration obtained from samples at the same frequency were accumulated and summed, as shown in Fig. 4b. The curves verify that the uranium leaching amount increases with increasing vibration time at a given vibration frequency during the layer leaching process.

3.1.2. Effect of vibration on HCO_3^- concentration

CO_2+O_2 leaching is essentially the process by which uranium is leached by HCO_3^-. The HCO_3^- concentration must therefore be determined. Standard acid solution was used to titrate HCO_3^- in the leaching solution (Asghar et al., 2020). The measured HCO_3^- concentrations are shown in Fig. 5. The ranges of HCO_3^- concentration are as follows: 363–1057.67 mg/L at 30 Hz, 359.49–1302.35 mg/L at 20 Hz, 428.29–1684.44 mg/L at 10 Hz, 304.79–900.43 mg/L at 28 kHz, and 328.38–977.61 mg/L at 40 kHz.

Fig. 5 shows that lower low-frequency vibrations are associated with higher HCO_3^- concentrations, whereas higher-frequency ultrasonic vibrations are associated with higher HCO_3^- concentrations. The HCO_3^- concentrations in solution under low-frequency vibration are also higher than those under ultrasonic vibration. This is mainly because the HCO_3^- concentration in Fig. 5 represents the ion concentration in solution after the reaction. Under the same gas pressure and temperature conditions, the same amount of CO_2 and O_2 dissolves in water. The low-frequency vibration only accelerates the equilibrium process of the dissolved gas, but does not affect the equilibrium result (Vreme et al., 2015). After the CO_2 and O_2 attained dissolution equilibration under the same inflation pressure and temperature conditions, the formed HCO_3^- concentrations are equivalent under different low-frequency vibration frequencies. Higher leaching content of uranium ions is associated with more consumption of HCO_3^- in solution and less residual

HCO_3^-. In contrast, ultrasonic vibration promotes dissolved CO_2 desorption in water (Jin et al., 2021), thus the HCO_3^- formed in solution is less than that under low-frequency vibration. This implies a higher leaching effect of low-frequency vibration than ultrasonic vibration. The leached uranium content of the 28 kHz treatment is higher than that of the 40 kHz treatment, thus the remaining HCO_3^- in solution in the former is less. The HCO_3^- concentration follows as 10 Hz > 20 Hz > 30 Hz > 40 kHz >28 kHz.

3.1.3. Effect of vibration on the other ions

Ca^{2+} and Mg^{2+} concentrations in solution under low-frequency vibration were determined using atomic adsorption spectrophotometry, and the curves shown in Fig. 6 represent the same vibration duration. Higher vibration frequencies are associated with higher Ca^{2+} and Mg^{2+} concentrations. The range of Ca^{2+} concentration changed from 84.17 to 328.66 mg/L at 10 Hz to 114.92–384.95 mg/L at 20 Hz and finally to 124.25–533.06 mg/L at 30 Hz. The range of Mg^{2+} concentration changed from 2.43 to 6.85 mg/L at 10 Hz to 2.69–7.1 mg/L at 20 Hz and finally to 3.56–7.29 mg/L at 30 Hz. For the same vibration frequency, Mg^{2+} concentrations tend to decrease with increasing vibration time, whereas Ca^{2+} concentrations increase. This is mainly because the experimental samples tested over different vibration times were matched and prepared from different ore samples. The samples contained less Mg^{2+}, thus the Mg^{2+} concentration decreased over time, whereas 104-g calcite was added, thus the Ca^{2+} concentration showed a rising trend.

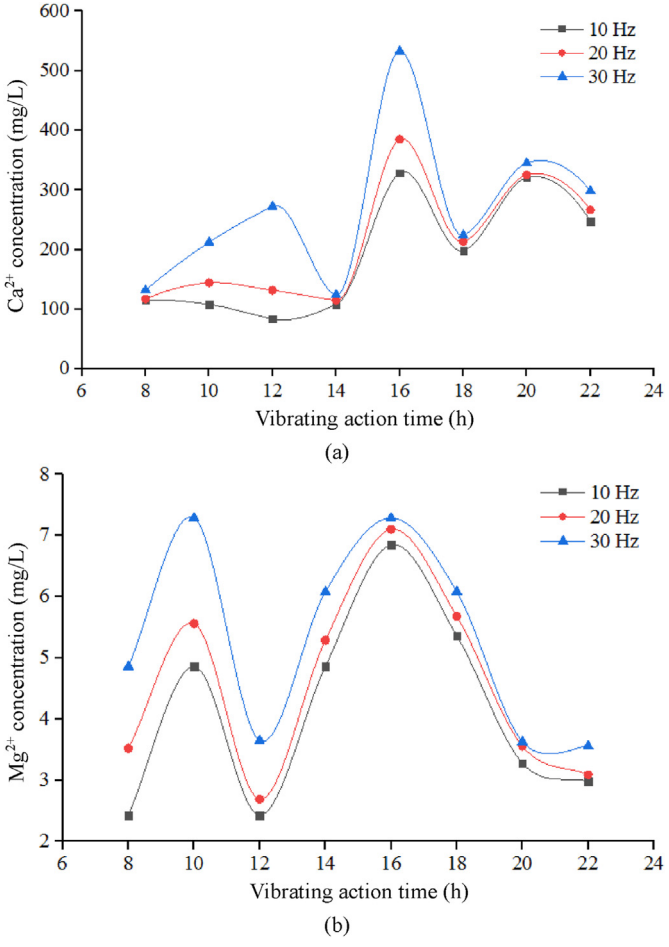

Fig. 6. (a) Ca^{2+} and (b) Mg^{2+} concentrations in solution variations after low-frequency vibration.

3.1.4. Effect of vibration on the permeability

The sample permeability was measured before and after low-frequency vibration. The permeability variation range before vibration was 0.05–1.98 mD, which is classified as a low-permeability sandstone. The change of permeability (i.e. post-vibration minus pre-vibration) is shown in Fig. 7. The variation range of the permeability increment was 0.098–0.982 mD at 10 Hz, 0.138–1.194 mD at 20 Hz, and 0.267–3.265 mD at 30 Hz. The results show that the permeability of the 30 Hz treated samples was 2.65–6.34 times higher than that of the untreated samples, 1.6–3.76 times higher than that of the 20 Hz treated samples, and 1.5–2.96 times higher than that of the 10 Hz treated samples. The results verify that low-frequency vibration effectively increases permeability and more so at higher vibration frequencies.

Similarly, the permeability of samples treated at the same frequency was accumulated and summed, as shown in Fig. 7b. The results show that the permeability increases with increasing vibration treatment time for a given frequency during the layer leaching process. Higher permeability changes are noted for higher-frequency treatments at a given vibration time during the layer leaching process.

3.1.5. Effect of vibration on sample erosion

The sample appearance was analyzed after 22 h of low-frequency vibration treatment to assess the erosion effect. The variation of the sample top and bottom surfaces are shown in Fig. 8 for samples treated under different vibration frequencies.

Fig. 8 shows that higher vibration frequencies are associated with more intense sample erosion. Under 10 Hz vibration treatment, the sample top surface showed protrusion and had slightly fallen off, and the bottom surface presented an erosion pit. Under 20 Hz vibration treatment, the top surface appeared notably uneven compared with that of the 10 Hz treatment and with more apparent protrusion, and the bottom surface had a deeper erosion pit that had partially fallen off. Under 30 Hz vibration treatment, the top and bottom surfaces both showed that a full layer had fallen off, with more severe erosion on the bottom surface than the top surface.

Faster diffusion at higher-vibration frequencies (or longer vibration treatment durations) disperses HCO_3^- produced by dissolved gas and ion concentrations produced by chemical erosion to ultimately become uniform in solution, which then leads to faster ion exchange between the solution and sandstone sample (Idiart et al., 2011; Ikumi et al., 2014; Qin et al., 2020). The chemical reaction rate thus increases and the sample is more seriously eroded, which is more conducive to the uranium leaching reaction and thus produces more uranium ions in solution.

3.2. Experimental comparison

Low-frequency vibration leaching studies have not been reported in the literature, whereas ultrasonic vibration leaching has been extensively studied. Ultrasound vibration was therefore selected to compare with the low-frequency vibration results obtained in this study. Low-frequency vibration and ultrasound waves are both mechanical vibrations. The low-frequency vibration ranges from 0.01 Hz to 100 Hz, whereas ultrasound frequencies are >20 KHz (Zhang et al., 2008a). The improvement mechanisms of the two vibration forms differ: low-frequency vibration only enhances physical action and influences the chemical reactions and permeability via physical vibration, whereas ultrasound treatment produces a cavitation effect (Avvaru et al., 2006, 2008; Ladola et al., 2014).

In previous ultrasonic vibration experiments, the leaching content was improved with vibration time (Avvaru et al., 2006, 2008;

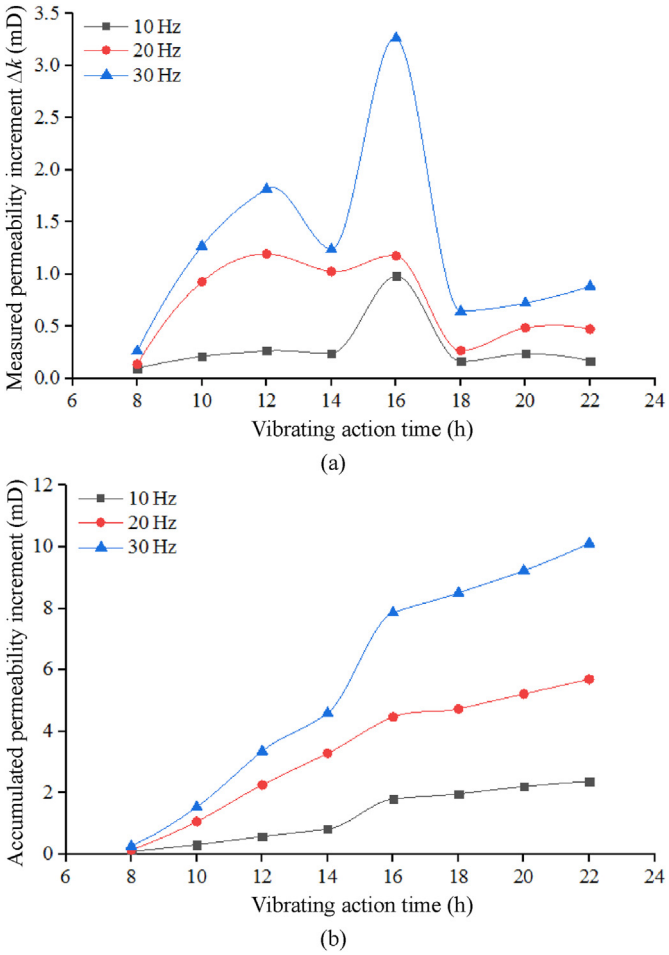

Fig. 7. Changes of (a) measured and (b) accumulated permeability increments under low-frequency vibration.

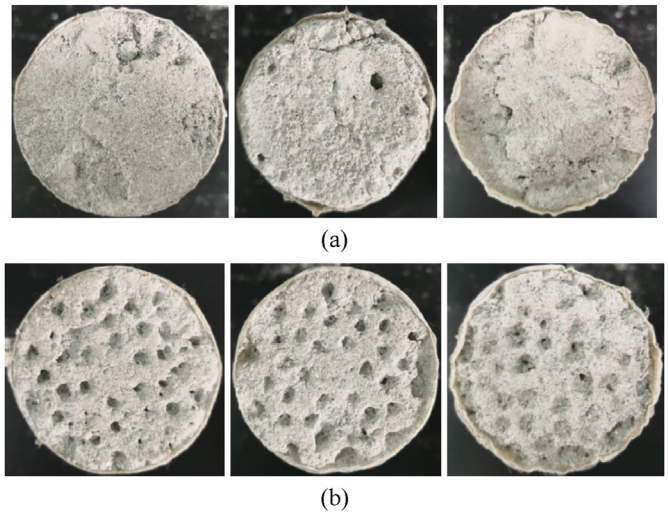

Fig. 8. (a) Top and (b) bottom surfaces for samples under vibration frequencies of 10 Hz, 20 Hz and 30 Hz after 22 h from the left to right.

Ladola et al., 2014), because identical particulate dispersion samples were used (Avvaru et al., 2006, 2008; Xue et al., 2010; Chen et al., 2015, 2020; Li et al., 2015, 2018; Zhang et al., 2016a; Wang et al., 2020). In this study, compressed and shaped samples were used to obtain low-permeability sandstone. Because gas was used as the leaching agent, undissolved high-pressure gas remained in the reaction kettle after the experiment. If the same sample was used at prolonged leaching times at the same frequency, it was not possible to consecutively obtain leaching solution without changing the experiment conditions. Single samples were thus used to continue the repeated experiment under the same experimental conditions. The vibration treatment time was thus fixed for samples prepared from a single drill hole, but varied between drill holes to return the original state of the actual underground leaching conditions as much as possible. The leaching content and permeability thus tended to fluctuate. However, the experiments were able to differentiate the effects of different vibration frequencies on the leaching content and permeability. The leaching content of a single sample was accumulated at a given frequency and variable vibration time, which better reflects the impact of vibration on sandstone leaching in practical layer leaching processes.

The results and analysis show that low-frequency vibration increases the permeability of low-permeability sandstone and effectively promotes chemical reactions, which enhance the effectiveness of uranium leaching. CO_2 and O_2 are inexpensive, nontoxic, and readily available. This controlled vibration approach emits no pollution into the environment, the resource utilization rate is substantially improved, and the waste of other resources is eliminated.

3.3. Permeability model

Permeability is a key factor responsible for low-permeability sandstone during uranium leaching. To further analyze the effect of low-frequency vibration on the permeability of low-permeability sandstone, it is necessary to establish a permeability model from a physical chemistry approach. During the CO_2+O_2 leaching process, the leaching solution flows into the sample pores and the reaction proceeds after contacting the sample, thus uranium in the samples dissolves into the leaching solution. Physico-chemical reactions occur simultaneously during this process. Under the action of low-frequency vibration, the flow of the solution accelerated by the vibration produces a stronger impact on the sample, which enhances the hydraulic erosion. After vibration, the internal pores of the sample and contact area between the solution and sample increase, thus the reaction becomes more intense. The influence of low-frequency vibration on leaching therefore includes the vibration impact on the sample and leaching solution.

Under low-frequency vibration, vibration waves are directly propagated into the sample interior and the sample porosity increases owing to the received physical vibration (Li et al., 2016). The sample is also impacted by the leaching solution, the porosity increases in response to the physical shocks, and erosion by the chemical action of the solution also occurs. The sample porosity is thus affected by the physical vibration of the vibration waves, physical shocks of the leaching solution, and hydrochemical action of the solution. The porosity of sandstone can be expressed as (Wei and Zhang, 2010; Kassab and Weller, 2011; Xu et al., 2020):

$$\varphi = \frac{V_P}{V_B} = \frac{V_{P\sigma} + V_{ch} + V_{P0}}{V_B} = 1 - \frac{1-\varphi_0}{1+\varepsilon_v}\left(1 + \frac{\Delta V_S}{V_{S0}}\right) = 1 - \frac{1-\varphi_0}{1+\varepsilon_v}\left[1 + \frac{\Delta V_{S\sigma}}{V_{S0}} + \frac{V_{ch}}{V_B(1-\varphi_0)}\right] \quad (4)$$

where V_B is the total sample volume (m^3), V_P is the sample pore volume (m^3), $V_{P\sigma}$ is the physical vibration pore volume (m^3), V_{ch} is the pore volume of chemical erosion (m^3), V_{P0} is the initial sample pore volume (m^3), ε_v is the volume strain, $\Delta V_{S\sigma}$ is the change of the skeleton volume caused by external vibration (m^3), V_{S0} is the initial

skeleton volume (m^3), φ_0 is the initial sample porosity, and φ is the sample porosity under vibration.

(1) Physical impact analysis

Under the impacts of mechanical vibration and water, the sample shows a change of extrusion volume $\Delta V_{s\sigma}$. The applied vibration exciter force during a half cycle can be expressed as (Li et al., 2016):

$$f_0 = \frac{2}{T_z}\int_0^{\frac{T_z}{2}} F\sin(2\pi\omega t)\mathrm{d}t = \frac{2F}{\pi} \tag{5}$$

where ω is the vibration frequency of the vibration source (Hz), F is the vibration force amplitude of the exciter (N), T_z is the vibration period (s), and t is the vibration time (s).

The vibration stress values of a half cycle in one direction are evenly distributed over a single cycle and the average vibration stress values of one cycle in this direction are obtained. The vibration stress values f received by the rock mass at time t can thus be expressed as (Li et al., 2016):

$$f = \frac{1}{2}\left[\frac{2}{T_z}\int_0^{\frac{T_z}{2}} F\sin(2\pi\omega t)\mathrm{d}t\right]\frac{t}{T_z} = \frac{F\omega t}{\pi} \tag{6}$$

The vibration stress f_s received by the sample within the reaction kettle at time t can be expressed as

$$\begin{aligned} f_s &= m_s a_s = \frac{m_s\sigma}{m_w + m_s} \\ &= \frac{m_s}{m_w + m_s}\frac{1}{2}\left[\frac{2}{T_z}\int_0^{\frac{T_z}{2}} F\sin(2\pi\omega t)\mathrm{d}t\right]\frac{t}{T_z} = \frac{F\omega t m_s}{\pi(m_w + m_s)} \end{aligned} \tag{7}$$

where a_s is the acceleration of sample (m/s), σ is the vibration force of the exciter in one cycle (N), m_w refers to the mass of the leaching solution in the reaction kettle (kg), and m_s is the mass of the sample in the reaction kettle (kg).

The sample in the reaction kettle is affected by the water impact force f_w, which can be expressed as

$$\begin{aligned} f_w &= m_w a_w = \frac{m_w\sigma}{m_w + m_s} = \frac{m_w}{m_w + m_s} \\ &\times \frac{1}{2}\left[\frac{2}{T_z}\int_0^{\frac{T_z}{2}} F\sin(2\pi\omega t)\mathrm{d}t\right]\frac{t}{T_z} = \frac{F\omega t m_w}{\pi(m_w + m_s)} \end{aligned} \tag{8}$$

where a_w is the acceleration of solution in the reaction kettle (m/s).

According to Eqs. (7) and (8), the stress σ_i received by the unit volume of sandstone sample can be expressed as

$$\sigma_i = \frac{f_s + f_w}{V_s} = \frac{1}{V_s}\frac{1}{2}\left[\frac{2}{T_z}\int_0^{\frac{T_z}{2}} F\sin(2\pi\omega t)\mathrm{d}t\right]\frac{t}{T_z} = \frac{F\omega t}{V_s\pi} \tag{9}$$

Ignoring the attenuation of stress waves, the skeleton volume strain $\Delta V_{s\sigma}/V_{s0}$ of the sample skeleton under mechanical vibration and water impact can be expressed as

$$\frac{\Delta V_{s\sigma}}{V_{s0}} = -\frac{f_w + f_s}{E_v} = -\frac{F\omega t}{\pi E_v} \tag{10}$$

where E_v is the sandstone bulk modulus (Pa).

(2) Chemical influence analysis

The main chemical reaction during the CO_2+O_2 leaching process is expressed as (Rao et al., 2014; Kim et al., 2014; Sreenivas and Chakravartty, 2016; Asghar et al., 2020; Shen et al., 2020):

$$2UO_2 + O_2 + 4HCO_3^- = 2[UO_2(CO_3)_2]^{2-} + 2H_2O \tag{11}$$

Because a large amount of calcite was added during the sample molding process, the chemical reaction that leads to the porosity change related to the increased amount of Ca^{2+} and Mg^{2+} in the leaching solution is expressed as (Li et al., 2018b):

$$CaCO_3 + CO_2 + H_2O = Ca^{2+} + 2HCO_3^- \tag{12}$$

$$CaMg(CO_3)_2 + 2CO_2 + 2H_2O = Ca^{2+} + Mg^{2+} + 4HCO_3^- \tag{13}$$

Eqs. (11)–(13) show that 1 mol of UO_2 generates 1 mol of $[UO_2(CO_3)_2]^{2-}$, 1 mol of $CaMg(CO_3)_2$ generates 1 mol of Mg^{2+} and 1 mol of Ca^{2+}, and 1 mol of $CaCO_3$ generates 1 mol of Ca^{2+}. A chemical erosion volume is thus formed by the dissolution of UO_2, $CaCO_3$ and $CaMg(CO_3)_2$, among which $CaCO_3$ generates a Ca^{2+} concentration equal to the Ca^{2+} concentration minus Mg^{2+} concentration in solution. The specific computation method is written as

$$\begin{aligned} V_{ch0} &= V_{ch1} + V_{ch2} + V_{ch3} = \frac{m_1}{\rho_1} + \frac{m_2}{\rho_2} + \frac{m_3}{\rho_3} \\ &= \frac{n_1 M_{r1}}{\rho_1} + \frac{n_2 M_{r2}}{\rho_2} + \frac{n_3 M_{r3}}{\rho_3} = \frac{V_r c_1 M_{r1}}{\rho_1} + \frac{V_r(c_2 - c_1)M_{r2}}{\rho_2} + \frac{V_r c_3 M_{r3}}{\rho_3} \end{aligned} \tag{14}$$

where V_{ch1}, V_{ch2} and V_{ch3} are the secondary pore volumes formed by the dissolution of $CaMg(CO_3)_2$, $CaCO_3$ and UO_2, respectively (m^3); m_1, m_2 and m_3 are the masses of $CaMg(CO_3)_2$, $CaCO_3$ and UO_2 dissolution, respectively (kg); ρ_1, ρ_2 andρ_3 are the densities of $CaMg(CO_3)_2$, $CaCO_3$ and UO_2, respectively (kg/m^3); V_r is the post-reaction solution (m^3); n_1, n_2 and n_3 are the mole amounts of $CaMg(CO_3)_2$, $CaCO_3$ and UO_2, respectively (mol); c_1, c_2 and c_3 are the measured concentrations of Mg^{2+}, Ca^{2+} and uranyl ions after the reaction, respectively (mol/L); and M_{r1}, M_{r2} and M_{r3} are the molecular weights of $CaMg(CO_3)_2$, $CaCO_3$ and UO_2, respectively.

During sandstone erosion processes, the pore volume of chemical erosion (V_{ch}) includes not only the erosion volume of calcium, magnesium and uranium ions, but also other ions. The value of V_{ch} is therefore 1–2 times the erosion volume sum of calcium, magnesium and uranium ions. Undissolved high-pressure gas remained in the reaction kettle after the experiment and the chemical reactions were conducted sufficiently. A value of two times the erosion volume sum of calcium, magnesium and uranium ions is therefore considered appropriate.

(3) Volume strain analysis

During the vibration process, the strain experienced by the sample is a combination of vibration fracture strain, water impact strain, and chemical erosion strain. Of these, the vibration fracture strain and water impact strain result from vibration stress. The volume strain can then be expressed as

$$\varepsilon_v = \varepsilon_{ch} + \varepsilon_f + \varepsilon_w = \frac{V_{ch}t}{V_C t_{ch}} + \frac{\sigma_i}{E_v} = \frac{V_{ch}t}{V_C t_{ch}} + \frac{F\omega t}{E_v\pi} \tag{15}$$

where t_{ch} is the total time of the chemical reaction (s), ρ_s is the apparent density of the sandstone (kg/m^3), and V_C is the initial total sample volume that participates in the reaction (m^3).

(4) Permeability analysis

An expression for the sample porosity variation can be determined by substituting Eqs. (10), (14) and (15) into Eq. (4):

$$\varphi = 1 - \frac{1-\varphi_0}{1+\varepsilon_v}\left[1 - \frac{F\omega t}{\pi E_v} - \frac{V_{ch}}{V_B(1-\varphi_0)}\right] = 1 - \frac{1-\varphi_0}{1+\left(\frac{2V_{ch0}t}{V_C t_{ch}} + \frac{F\omega t}{E_v \pi}\right)}\left[1 - \frac{F\omega t}{\pi E_v} - \frac{2V_{ch0}}{V_B(1-\varphi_0)}\right] \quad (16)$$

An understanding of the relationship between permeability and porosity is required to determine the law of permeability variation, given as (Li et al., 2019; Wang et al., 2012; Zhang et al., 2008b):

$$k = k_0\left(\frac{\varphi}{\varphi_0}\right)^3 \quad (17)$$

where k is the sandstone permeability under vibration (mD) and k_0 is the initial permeability of sandstone. An expression for sample permeability during the leaching process can be determined by substituting Eq. (16) into Eq. (17).

The concentrations of uranyl ions, HCO_3^-, Ca^{2+} and Mg^{2+} and experimental parameters are substituted into Eqs. (16) and (17) to test the established permeability model. The calculated permeability variation is shown in Fig. 9. The experimental parameters are listed in Table 1.

A comparison of Figs. 7 and 9 shows that the established permeability model can accurately represent the measured permeability variations. To further examine the calculation accuracy, the accumulated permeability increment curves of the calculated and measured values are linearly fitted under the same frequency, as shown in Fig. 10. The fitting equation of the calculated values at 10 Hz is $y = -3.50837 + 0.39666x$ with the correlation coefficient of 0.92832. The fitted equation of the measured values at 10 Hz is $y = -1.46024 + 0.18195x$ with the correlation coefficient of 0.94397. This shows that there is a certain difference between the calculated and measured values in Fig. 10a; however, these values are consistent during 8–14 h of treatment duration, with differences appearing between 16 h and 22 h. The fitting equation of the calculated values at 20 Hz is $y = -4.09261 + 0.47151x$ with the correlation coefficient of 0.94659. The fitting equation of the measured values at 20 Hz is $y = -2.73327 + 0.40603x$ with the correlation coefficient of 0.95394. This shows that the calculated values in Fig. 10b essentially coincide with the measured values. The fitting equation of the calculated values at 30 Hz is $y = -5.79073 + 0.69577x$ with the correlation coefficient of 0.96372. The fitting equation of the measured values at 30 Hz is $y = -5.57512 + 0.75038x$ with the correlation coefficient of 0.95974. This shows that the calculated values in Fig. 10c were almost exactly consistent with the measured values. The above comparison shows that the developed model can obtain comparatively accurate accumulated permeability increment values.

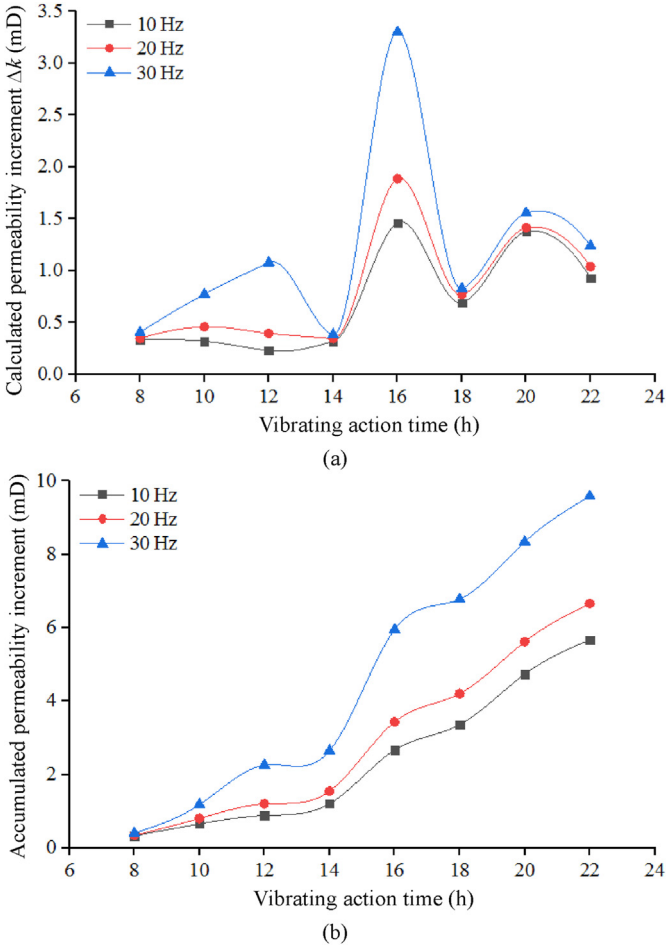

Fig. 9. Changes of (a) calculated and (b) accumulated permeability increments under low-frequency vibration.

Table 1
Experimental parameters.

Parameter	Value
Initial elastic modulus of sandstone, E (Pa)	4.35×10^{10}
Poisson ratio, ν	0.25
Total volume of sandstone sample before reaction, V_C (m^3)	1.9635×10^{-4}
Overall reaction time, t_{ch} (s)	Value to be consistent with vibration time
Amplitude of driving force, F (N)	1 (measured)
Initial porosity of sandstone sample, φ_0	0.0132 (average value)
Sandstone sample quality affected by stress wave, m_s (kg)	0.429
Apparent density, ρ_s (kg/m^3)	2.1849×10^3
Vibration frequency, ω (Hz)	10, 20, 30
Testing temperature, T (°C)	30
Initial permeability, k (mD)	0.2994 (average value)

4. Conclusions

Low-frequency mechanical vibration was innovatively applied to the CO_2+O_2 leaching process of low-permeability sandstone to alter its permeability and increase the amount of leached uranium. The specific conclusions are as follows:

(1) A method for uranium leaching is proposed that can significantly increase the leaching efficiency from low-permeability sandstone. The testing system for vibration leaching was independently developed.

(2) The results show that low-frequency vibration significantly improves the uranium leaching performance and permeability of low-permeability sandstone samples. The enhanced leaching effect produced by low-frequency vibration treatment is superior to that of ultrasonic vibration. During 22 h of leaching, the uranium leaching content

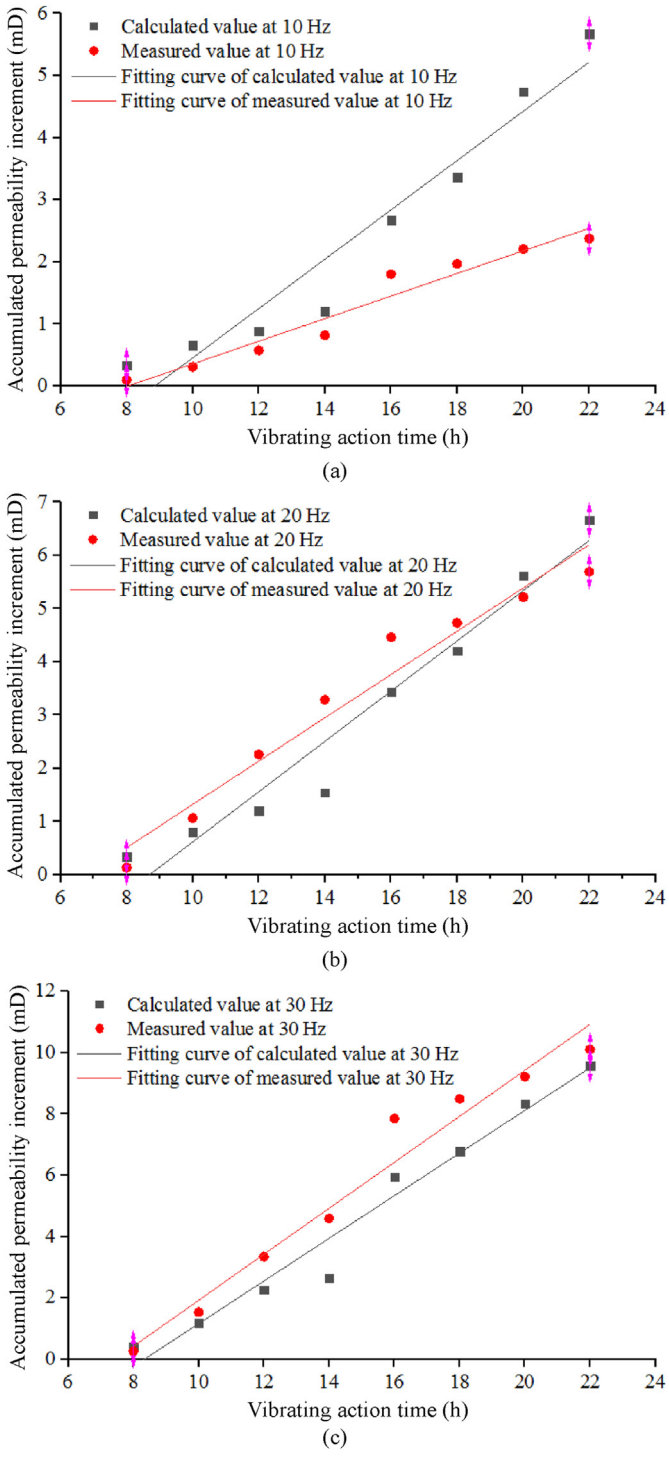

Fig. 10. Fitting curves of the accumulated permeability increment under low-frequency vibration: (a) 10 Hz, (b) 20 Hz, and (c) 30 Hz.

reached up to 2.36 mg/L under low-frequency vibration treatment; 9 times higher than that obtained under ultrasonic vibration (0.257 mg/L), whereas the concentration of uranium ions generated without vibration treatment was not detectable. The initial sample permeability (0.05–1.98 mD) increased by 0.267–3.265 md following the low-frequency vibration treatment.

(3) A mathematical model that accounts for the effect of low-frequency vibration on permeability was established considering the combined action of physico-mechanical vibration and chemical erosion. The results show good consistency between the calculated and measured permeability values.

Although the laboratory results presented here are preliminary, they provide important guidelines for future industrial production.

Declaration of competing interest

The authors declare that they have no known competing financial interests or personal relationships that could have appeared to influence the work reported in this paper.

Acknowledgments

This work was sponsored by the National Natural Science Foundation of China (Grant No. 11705086), Natural Science Foundation of Hunan Province (Grant No. 2018JJ3424), and Fund of Hunan Provincial Department of Education (Grant No. 16C1387).

References

Ai, C.M., Sun, P.P., Wu, A.X., Chen, X., Liu, C., 2019. Accelerating leaching of copper ore with surfactant and the analysis of reaction kinetics. Int. J. Miner. Metall. Mater. 26, 274–281.
Avvaru, B., Roy, S.B., Chowdhury, S., Hareendran, K.N., Pandit, A.B., 2006. Enhancement of the leaching rate of uranium in the presence of ultrasound. Ind. Eng. Chem. Res. 45 (22), 7639–7648.
Avvaru, B., Roy, S.B., Ladola, Y., Chowdhury, S., Hareendran, K.N., Pandit, A.B., 2008. Sono-chemical leaching of uranium. Chem. Eng. Process 47 (12), 2107–2113.
Asghar, F., Sun, Z.X., Chen, G.X., Zhou, Y.P., Li, G.R., Liu, H.Y., Zhao, K., 2020. Geochemical characteristics and uranium neutral leaching through a CO_2+O_2 system - an example from uranium ore of the ELZPA ore deposit in Pakistan. Metals 10 (12), 1616.
Cai, G.L., Tan, K.X., Wang, W.G., 2013. Effect of different surfactant on leaching of uranium in sandstone type ores with low permeability. Adv. Mater. Res. 2203 (634), 3335–3338.
Cho, K., Kim, H., Myung, E., Purev, O., Choi, N., Park, C., 2020. Recovery of gold from the refractory gold concentrate using microwave assisted leaching. Metals 10 (5), 571.
Chen, N., Cao, Z.F., Zhong, H., Fan, F., Qiu, P., Wang, M.M., 2015. A novel approach for recovery of nickel and iron from nickel laterite ore. Metall. Res. Technol. 112 (3), 306–318.
Chen, B., Bao, S.X., Zhang, Y.M., Li, S., 2020. A high-efficiency and sustainable leaching process of vanadium from shale in sulfuric acid systems enhanced by ultrasound. Separ. Purif. Technol. 240 (1), 116624.
Deng, R.R., Xie, Z.M., Liu, Z.H., Tao, C.Y., 2019. Leaching kinetics of vanadium catalyzed by electric field coupling with sodium persulfate. J. Electroanal. Chem. 854, 113542.
Du, R.K., Zhang, X.W., Li, M., Wu, X.Y., Liu, Y., Jiang, T.J., Chen, C., Peng, Y., 2019. Leaching of low permeable sandstone uranium ore using auxiliary materials: anionic surfactants. J. Radioanal. Nucl. Chem. 322 (2), 839–846.
Idiart, A.E., López, C.M., Carol, I., 2011. Chemo-mechanical analysis of concrete cracking and degradation due to external sulfate attack: a meso-scale model. Cement Concr. Compos. 33 (3), 411–423.
Ikumi, T., Cavalaro, S.H.P., Segura, I., Aguado, A., 2014. Alternative methodology to consider damage and expansions in external sulfate attack modeling. Cement Concr. Res. 63, 105–116.
Jin, F.Q., Xu, H.P., Hua, D.L., Chen, L., Li, Y., Zhao, Y.X., Zuo, B., 2021. Enhancement of CO_2 desorption using ultrasound and vacuum in water scrubbing biogas upgrading system. Kor. J. Chem. Eng. 38 (1), 129–134.
Kim, J.H., Cho, H.C., Han, K., 2014. Leaching behavior of U and V from a Korean uranium ore using Na_2CO_3 and KOH. Geosystem Eng 17 (2), 113–119.
Kassab, M.A., Weller, A., 2011. Porosity estimation from compressional wave velocity: a study based on Egyptian sandstone formations. J. Petrol. Sci. Eng. 78, 310–315.
Laubertova, M., Havlik, T., Parilak, L., Derin, B., Trpcevska, J., 2020. The effects of microwave-assisted leaching on the treatment of electric arc furnace dusts (EAFD). Arch. Metall. Mater. 1 (65), 321–328.
Ladola, Y.S., Chowdhury, S., Roy, S.B., Pandit, A.B., 2014. Application of cavitation in uranium leaching. Desalination Water Treat. 52 (1–3), 407–414.
Li, S.W., Chen, W.H., Yin, S.H., Ma, A.Y., Yang, K., Xie, F., Zhang, L.B., Peng, J.H., 2015. Impacts of ultrasound on leaching recovery of zinc from low grade zinc oxide ore. Green Process. Synth. 4 (4), 323–328.

Li, S.G., Zhao, Y., Xu, M.G., 2016. Gas porosity formula under low frequency vibration and its testing analysis. J. China Coal Soc. 41 (10), 2612–2619.
Li, H.Y., Li, S.W., Srinivasakannan, C., Zhang, L.B., Yin, S.H., Yang, K., Xie, H.M., 2018a. Efficient cleaning extraction of silver from spent symbiosis lead-zinc mine assisted by ultrasound in sodium thiosulfate system. Ultrason. Sonochem. 49, 118–127.
Li, S.G., Huo, R.K., Wang, B., Ren, Z.Z., Ding, Y., Qian, M.T., Qiu, T., 2018b. Experimental study on physicomechanical properties of sandstone under acidic environment. Adv. Civ. Eng. 2018, 5784831.
Li, B., Liang, Y.P., Zhang, L., Zou, Q.L., 2019. Experimental investigation on compaction characteristics and permeability evolution of broken coal. Int. J. Rock Mech. Min. Sci. 118, 63–76.
Li, M., Gao, F.Y., Zhang, X.W., Lv, S.Y., Huang, J., Wu, X.Y., Fang, Q., 2020. Recovery of uranium from low-grade tailings by electro-assisted leaching. J. Clean. Prod. 271 (1), 122639.
Makaryuk, N.V., 2009. Seismic vibration treatment of a pay zone for improvement of the filtration and production parameters of underground metal leaching. J. Min. Sci. 45 (6), 590–601.
Mudd, G.M., 2001. Critical review of acid in situ leach uranium mining: 1. USA and Australia. Environ. Geol. 41 (3/4), 390–403.
Pan, W., Jin, H.M., Liu, Z.Z., Tang, J.H., Cheng, S.Y., 2020. Experimental and theoretical study on strengthening leaching of sulfide ores by surfactants. Process Saf. Environ. Protect. 137, 289–299.
Qin, S.S., Zou, D.J., Liu, T.J., Jivkov, A., 2020. A chemo-transport-damage model for concrete under external sulfate attack. Cement Concr. Res. 132, 106048.
Rao, K.A., Sreenivas, T., Vinjamur, M., Suri, A.K., 2014. Continuous leaching of uranium from an Indian ore: residence time scale up and heat effects. Hydrometallurgy 146, 119–127.
Shen, N., Li, J., Guo, Y.F., Li, X.C., 2020. Thermodynamic modeling of in situ leaching of sandstone-type uranium minerals. J. Chem. Eng. Data 65 (4), 2017–2031.
Sreenivas, T., Chakravartty, J.K., 2016. Alkaline processing of uranium ores of Indian origin. Trans. Indian Inst. Met. 69 (1), 3–14.
Sun, Q., Retnanto, A., Amani, M., 2020. Seismic vibration for improved oil recovery: a comprehensive review of literature. Int. J. Hydrogen Energy 45 (29), 14756–14778.
Tan, K.X., Li, C.G., Liu, J., Qu, H.Q., Xia, L.S., Hu, Y., Li, Y.M., 2014. A novel method using a complex surfactant for in-situ leaching of low permeable sandstone uranium deposits. Hydrometallurgy 150, 99–106.
Tian, Y., Shu, J.C., Chen, M.J., Wang, J.Y., Wang, Y., Luo, Z.G., Wang, R., Yang, F.H., Xiu, F.R., Sun, Z., 2019. Manganese and ammonia nitrogen recovery from electrolytic manganese residue by electric field enhanced leaching. J. Clean. Prod. 236, 117708.
Vreme, A., Pouligny, B., Nadal, F., Liger-Belair, G., 2015. Does shaking increase the pressure inside a bottle of champagne. J. Colloid Interface Sci. 439 (1), 42–53.
Wang, J.G., Kabir, A., Liu, J.S., Chen, Z.W., 2012. Effects of non-Darcy flow on the performance of coal seam gas wells. Int. J. Coal Geol. 93, 62–74.
Wang, Y.D., Li, G.Y., Ding, D.X., Zhou, Z.X., Deng, Q.W., Hu, N., Tan, Y., 2013. Uranium leaching using mixed organic acids produced by Aspergillus Niger. J. Radioanal. Nucl. Chem. 298 (2), 769–773.
Wang, J.X., Faraji, F., Ghahreman, A., 2020. Effect of ultrasound on the oxidative copper leaching from chalcopyrite in acidic ferric sulfate media. Minerals 10 (7), 633.
Wei, Z.J., Zhang, D.X., 2010. Coupled fluid-flow and geomechanics for triple-porosity/dual-permeability modeling of coalbed methane recovery. Int. J. Rock Mech. Min. Sci. 47 (8), 1242–1253.
Xu, D.D., Tao, Y.Q., Zhou, Z.T., Hou, C., 2020. Study of the law of hydraulically punched boreholes on effective gas extraction radius under different coal outputs. Shock Vib. 8858091, 2020.
Xue, J.Q., Lu, X., Du, Y.W., Mao, W.B., Wang, Y.J., Li, J.X., 2010. Ultrasonic-assisted oxidation leaching of nickel sulfide concentrate. Chin. J. Chem. Eng. 18 (6), 948–953.
Yang, Y., Ram, R., McMaster, S.A., Pownceby, M.I., Chen, M., 2020. A comparative bio-oxidative leaching study of synthetic U-bearing minerals: implications for mobility and retention. J. Hazard Mater. 403, 123914.
Ye, L.Z., Zhu, X.J., Liu, Y., 2019. Numerical study on dual-frequency ultrasonic enhancing cavitation effect based on bubble dynamic evolution. Ultrason. Sonochem. 59, 104744.
Yuan, W., Wang, W., Su, X.B., Li, J.X., Li, Z.H., Wen, L., Chang, J.F., 2018. Numerical study of the impact mechanism of decoupling charge on blasting-enhanced permeability in low-permeability sandstones. Int. J. Rock Mech. Min. Sci. 106, 300–310.
Zhang, J., Wu, A.X., Wang, Y.M., Chen, X.S., 2008a. Experimental research in leaching of copper-bearing tailings enhanced by ultrasonic treatment. J. China Univ. Min. Technol. 18 (1), 98–102.
Zhang, H.B., Liu, J.S., Elsworth, D., 2008b. How sorption-induced matrix deformation affects gas flow in coal seams: a new FE model. Int. J. Rock Mech. Min. Sci. 45 (8), 1226–1236.
Zhang, L.B., Guo, W.Q., Peng, J.H., Li, J., Lin, G., Yu, X., 2016a. Comparison of ultrasonic-assisted and regular leaching of germanium from by-product of zinc metallurgy. Ultrason. Sonochem. 31, 143–149.
Zhang, Y.F., Ma, J.Y., Qin, Y.H., Zhou, J.F., Yang, L., Wu, Z.K., Wang, T.L., Wang, W.G., Wang, C.W., 2016b. Ultrasound-assisted leaching of potassium from phosphorus-potassium associated ore. Hydrometallurgy 166, 237–242.
Zhao, Z.W., Ding, W.T., Liu, X.H., Liang, y., 2013. Effect of ultrasound on kinetics of scheelite leaching in sodium hydroxide. Can. Metall. Q. 52 (2), 138–145.
Zhu, P., Zhang, X.J., Li, K.F., Qian, G.R., Zhou, M., 2012. Kinetics of leaching refractory gold ores by ultrasonic-assisted electro-chlorination. Int. J. Miner. Metall. Mater. 19 (6), 473–477.

Yong Zhao obtained his BSc degree in Mining Engineering from Henan Polytechnic University, China, in 2008, his MSc and PhD degrees in Safety Technology and Engineering from Xi'an University of Science and Technology, China, in 2011 and 2014, respectively. He was employed by University of South China as Lecturer. Currently, he is performing the postdoctoral work at China Institute of Atomic Energy. His research interests cover laboratory testing, nuclear waste disposal, radioactive nuclide migration, constitutive modeling, environmental geotechnics, etc.